Balanced multi-image demons for non-rigid registration of magnetic resonance images

Balanced Multi-Image Demons for Non-Rigid Registration of Magnetic Resonance Images

Luca Mesin[a,*]

[a] *Mathematical Biology and Physiology, Dept. Electronics and Telecommunications, Politecnico di Torino, Turin, Italy*

Abstract

A new approach is introduced for non-rigid registration of a pair of magnetic resonance images (MRI). It is a generalization of the demons algorithm with low computational cost, based on local information augmentation (by integrating multiple images) and balanced implementation. Specifically, a single deformation that best registers more pairs of images is estimated. All these images are extracted by applying different operators to the two original ones, processing local neighbors of each pixel. The following five images were found to be appropriate for MRI registration: the raw image and those obtained by contrast-limited adaptive histogram equalization, local median, local entropy and phase symmetry. Thus, each local point in the images is supplemented by augmented information coming by processing its neighbor. Moreover, image pairs are processed in alternation for each iteration of the algorithm (in a balanced way), computing both a forward and a backward registration.

The new method (called balanced multi-image demons) is tested on sagittal MRIs from 10 patients, both in simulated and experimental conditions, improving the performances over the classical demons approach with minimal increase of the computational cost (processing time around twice that of standard demons). Specifically, a simulated deformation was applied to the MRIs (either original or corrupted by additive Gaussian or speckle noises). In all tested cases, the new algorithm improved the estimation of the simulated deformation (squared estimation error decreased by about 65% in the average). Moreover, statistically significant improvements were obtained in experimental tests, in which different brain regions (i.e., brain, posterior fossa and cerebellum) were identified by the atlas approach and compared to those manually delineated (in the average, Dice coefficient increased of about 6%).

The conclusion is that a balanced method applied to multiple information extracted from neighboring pixels is a low cost approach to improve registration of MRIs.

Keywords: Demons, magnetic resonance imaging, non-rigid registration

*Corresponding author

Email address: luca.mesin@polito.it (Luca Mesin)

1. Introduction

Image registration estimates a transformation aligning the pixels of different images. It is useful to match pictures taken from the same object at different times [1], or from different viewpoints or sensors [2][3][4][5]. It can also be applied to images taken from different objects, to match them optimally in order to better compare them. The different images could be assumed to be related by either a simple rigid transformation (e.g., translation, rotation, affine transformation [6]) or a non-rigid deformation [3][4]. For each of these hypotheses, different methods have been proposed to estimate the transformation [2][4]. Image registration found many applications, e.g., in computer vision [7] and medical imaging [4][5][8], e.g., for the segmentation of the human brain [9][10][11][12][13][14][15].

Different approaches have been explored for non-rigid image registration [4], e.g., physical constraints [16], statistical models [15][17], deep learning [1][18]. Demons method is a non-parametric, non-rigid image registration technique which is appreciated for the good performances and low computational cost [19][20]. It is based on a diffusion process [4]. To match two images, the following interpretation was proposed (from which the method takes the name): object boundaries in one picture are like as semi-permeable membranes through which the other image, considered as a deformable grid model, diffuses thanks to local forces impressed by demons situated within them. Intensity variations across these object boundaries (i.e., polarity) drive diffusion. In practice, the gradient of the image intensity indicates the normal to object boundaries along which the deformable model is pushed to match the two images. The use of polarity was indicated as an important difference with respect to many other registration methods based on attraction, which instead relies on the concept of distance [19].

Some methods have been proposed to improve demons performances, e.g., by processing multiple recorded images [21][22] or imposing the registration to be symmetric [23], but they have quite a high computational cost [24][25].

In this paper, a new algorithm is proposed to improve demons registration still keeping a low computational cost, based on local information augmentation (by integrating multiple images) and balanced implementation. Specifically, the idea is to generalize demons algorithm to process together more image pairs obtained by pre-processing the two pictures to be registered and to treat them in a balanced way. As all images are extracted from the same original ones, they are assumed to be affected by the same deformation, which is estimated optimally in the least mean squared sense. All these images have the same dimensions as the original ones from which they were obtained. They are produced by filtering or texture processing operations, each extracting some feature of the objects represented in the images (which should be significant for improving the registration). These processing procedures apply locally, extracting some specific information (depending on the operation applied) from a neighbor of each pixel.

Notice that, in general, the assumption that a single transformation matches all image pairs cannot be strictly satisfied, as the deformation changes the neighbors of the pixels, affecting the result of the filtering operators generating the pairs of images. However, it is expected that, by extracting meaningful features and including a sufficient number of images in the sets, the beneficial effect of integrating their information can emerge.

It is claimed that integrating information from such images could be considered as a multi-modal approach that is similar to the way in which images are interpreted by intel-

ligent individuals: indeed, when a person is looking at a specific direction, each visualized point is not investigated out of its context, but specific properties (e.g., local symmetry, homogeneity, roughness, texture, anisotropy,...) are associated to each location to decode the scene.

The registration problem is iteratively linearized and the update is computed analytically, thus getting a fast algorithm. Moreover, the update is applied alternatively to each of the two sets of images, obtaining a balanced method in which each one is given the same importance.

In the following sections, the method is described in details and optimized for magnetic resonance images (MRI). It is then tested in simulated conditions (i.e., estimating a specific deformation applied on an MRI, possibly corrupted by noise) and in a typical experimental problem (i.e., identifying brain regions using the atlas approach [26][27][28][29]).

2. Materials and Methods

2.1. Image acquisition and preparation

Ten pediatric patients with Chiari malformation were considered. Sagittal T1-weighted head MRIs were acquired at 1.5 Tesla (the first 10 subjects of the dataset discussed in [30][31] were selected). Data were digitally sampled on a matrix of 256×256 pixels and saved in DICOM format.

The images were first registered by an affine transformation, in order to match nasion and inion. Then, they were converted into gray-scale and adjusted to span all 256 levels. The lowest level was assigned to the background, automatically estimated by global thresholding, selecting the threshold as the first local minimum in the histogram of the image (smoothed by a median filter with neighbor of 5×5 pixels).

Both simulated and experimental conditions (detailed below) were considered to make tests of registration.

2.1.1. Simulated deformation

Each MRI was processed by a known deformation (specifically, two images were randomly selected and registered by the classical demons algorithm; the obtained deformation was enlarged by 50%). The algorithm was then applied to estimate such a simulated deformation and the mean squared error was used to quantify the performances. Only the region including the head was considered to estimate the error, as large mistakes could be tolerated in the background surrounding it.

Tests were repeated on the same images after corrupting them with noise. Two noisy perturbations were used to corrupt the two images before registration: additive Gaussian noise with zero mean and standard deviation equal to 0.2% of the maximum intensity of the image; speckle noise, i.e., the image was multiplied by $(1 + n)$, where n is uniformly distributed with zero mean and variance 0.04. For each image and each type of noisy perturbation, 10 realizations were considered. Thus, a total number of 210 simulations were obtained (10 noise-free deformations for each of the 10 MRIs; 100 cases for each of the two types of noise). An example of MRI (either noise free or perturbed) is shown in Figure 1.

2.1.2. Delineation of brain regions

The experimental problem of identifying some brain regions by registration over an atlas [26][27][28][29] was considered. The brain, posterior fossa and cerebellum were delineated over each of the 10 MRIs. Then the 3 regions were automatically delineated by registration over an atlas. Each image was considered in turn as the atlas and was used to register each of the other images. In this way, 90 tests were performed in total. The estimated regions were compared to the ones delineated manually, using the following overlapping error

$$E_O(M_T, M_E) = 2\frac{|M_T \setminus M_E| + |M_E \setminus M_T|}{|M_T| + |M_E|} \tag{1}$$

where M_T and M_E are the true (manually delineated) and estimated masks, respectively, $|\cdot|$ indicates the cardinality, $\setminus$ is the set difference (so that $|M_X \setminus M_Y|$ is the number of pixels belonging to the region in X which are not matched in Y).

2.2. Image processing

Demons algorithm is an important approach for image registration [32]. A short introduction to the method is first given. Then, the innovative variations proposed in this paper are detailed.

2.2.1. Introduction to Demons algorithm

The classical demons algorithm is here described, to introduce the notation and the ideas which are then extended to solve its multi-image and balanced generalizations. Consider the registration of two images, each defined as a function of the point or pixel p: the target $F(p)$ (or deformed, or fixed) and the source $M(p)$ (original, or moving) images. The registration problem consists in estimating the deformation $s : p \to s(p)$ such that the deformed source image $M \circ s(p)$ matches $F(p)$, i.e., it minimizes a functional measuring dissimilarity. The mean squared error is considered as the functional to be minimized, so that the optimization problem is written as

$$\underset{s}{\operatorname{argmin}} \|F(p) - M \circ s(p)\|^2 \tag{2}$$

where $\|\cdot\|$ is the L_2 norm. This is not a well-posed problem, as its solution could be unstable (due to discretization, quantization and noise in the images). Some a-priori information is then introduced imposing constraints. To enforce the deformation to be regular, a penalization term involving its gradient is introduced

$$\underset{s}{\operatorname{argmin}} \frac{1}{\sigma_i^2} \|F(p) - M \circ s(p)\|^2 + \frac{1}{\sigma_T^2} \|\nabla s\|^2 \tag{3}$$

where ∇ indicates the gradient operator; σ_i and σ_T are parameters accounting for image noise and regularization, respectively. As the solution of this problem is not computationally efficient [32], a hidden variable c (of correspondences) is introduced, requiring to be an approximation of the transformation s accommodating possible errors. The problem is thus written as

$$\underset{s,c}{\operatorname{argmin}} \frac{\|F(p) - M \circ c(p)\|^2}{\sigma_i^2} + \frac{\|c(p) - s(p)\|^2}{\sigma_x^2} + \frac{\|\nabla s(p)\|^2}{\sigma_T^2} \tag{4}$$

where σ_x weights the spatial uncertainty in the correspondences.
This problem is iteratively solved in two steps: minimizing the sum of the first two terms with respect to c keeping s fixed and minimizing the sum of the last two terms with respect to s with c fixed. The second step can be solved analytically: s is obtained as a Gaussian smoothing of c (a standard deviation of 1.5 pixels is used in this paper). The first step is more involved and is tackled by the iterative solution of a local linearization problem. Assuming $c = s \circ (\mathbb{1} + u)$, where $\mathbb{1}$ is the identity map and u is a small deformation, the following linear approximation is obtained

$$\begin{aligned} &F(p) - M \circ c(p) = F(p) - M \circ s(p) \circ (\mathbb{1} + u(p)) \approx \\ &\approx F(p) - M \circ s(p) - J_p u(p) \end{aligned} \tag{5}$$

where J_p is the Jacobian operator of $M \circ s$ in the point p. The minimization problem is

$$\begin{aligned} &\underset{c}{\operatorname{argmin}} \tfrac{1}{\sigma_i^2} \left\| F - M \circ c \right\|^2 + \tfrac{1}{\sigma_x^2} \left\| c - s \right\|^2 = \\ &= \underset{u}{\operatorname{argmin}} \tfrac{1}{\sigma_i^2} \left\| F(p) - M \circ s \circ (\mathbb{1} + u) \right\|^2 + \tfrac{1}{\sigma_x^2} \left\| u \right\|^2 \approx \\ &\approx \underset{u}{\operatorname{argmin}} \tfrac{1}{\sigma_i^2} \left\| F(p) - M \circ s - J_p u \right\|^2 + \tfrac{1}{\sigma_x^2} \left\| u \right\|^2 \end{aligned} \tag{6}$$

to be solved separately for each point p. The functional to be minimized can be written in matrix form

$$\left\| F(p) - M \circ s - J_p u \right\|^2 + \frac{\sigma_i^2}{\sigma_x^2} \left\| u \right\|^2 = \left\| \begin{bmatrix} J_p \\ \frac{\sigma_i}{\sigma_x} \end{bmatrix} u - \begin{bmatrix} F(p) - M \circ s \\ 0 \end{bmatrix} \right\|^2 \tag{7}$$

The solution is obtained by pseudo-inversion as follows

$$\begin{aligned} &\begin{bmatrix} J_p^T & \frac{\sigma_i}{\sigma_x} \end{bmatrix} \begin{bmatrix} J_p \\ \frac{\sigma_i}{\sigma_x} \end{bmatrix} u = \begin{bmatrix} J_p^T & \frac{\sigma_i}{\sigma_x} \end{bmatrix} \begin{bmatrix} F(p) - M \circ s \\ 0 \end{bmatrix} \rightarrow \\ &\rightarrow \left(J_p^T J_p + \tfrac{\sigma_i^2}{\sigma_x^2} \right) u = (F(p) - M \circ s) J_p^T \rightarrow \\ &\rightarrow u = \tfrac{(F - M \circ s) J_p^T}{\left\| J_p \right\|^2 + \frac{\sigma_i^2}{\sigma_x^2}} \end{aligned} \tag{8}$$

The last expression is very similar to what could be obtained by another classical method for image registration: optical flow [33]. Indeed, assume to write $m = M \circ s$ in the arbitrary point p as a local linear approximation of F

$$F(p) \approx m(p) + J_p \vec{v}(p) = m + \nabla m \cdot \vec{v} \tag{9}$$

where $\vec{v}$ is a vector field indicating the optical flow that allows to map m into F. The previous equation can be written as

$$\nabla m \cdot \vec{v} = F - m \tag{10}$$

Assume the vector field to be aligned to the gradient of m (the orthogonal component cannot be determined, as its product with ∇m is always zero; this is called aperture problem). Then, it can be written as

$$\vec{v} = \frac{(F - m) \nabla m}{|\nabla m|^2} \tag{11}$$

This expression is unstable in points in which the gradient of m is small, so that a regularization was suggested [19]

$$\vec{v} = \frac{(F-m)\nabla m}{|\nabla m|^2 + (F-m)^2} \tag{12}$$

This expression is the same as (8) if the second term in the denominator σ_i^2/σ_x^2 is assumed to be equal to the mean squared approximation error $|F - M \circ s|^2$. This means that in each point a different regularization is considered, depending on the approximation error (so that σ_i^2/σ_x^2 is a function of the pixel p). In the following, we'll make this assumption.

The direct composition of more updates obtained by the demons algorithm would not lead to a smooth and invertible deformation, in general. Then, it is performed as suggested in [32], where the deformation was searched in the space of diffeomorphisms (i.e., smooth and invertible transformations, with smooth inverse). This allows to preserve object topology, avoiding not physical foldings. Specifically, once the update u is computed, it is projected onto the group of diffeomorphisms through the exponential map: thus, instead of computing $c = s \circ (\mathbb{1} + u)$ as above, the deformation is updated as $c = s \circ exp(u)$ (notice that the two expressions are the same at a first order of approximation). In order to compute the exponential map, notice that its application is equivalent to solving the following ordinary differential equation problem (applying the deformation u to the pixels, starting from the initial condition p_0)

$$\begin{cases} \frac{dp(t)}{dt} = u(p(t)) \\ p(0) = p_0 \end{cases} \tag{13}$$

and selecting $p(1) \equiv exp(u)$. Thus, the exponential transformation of an arbitrary point p is obtained as the solution at $t = 1$ of this equation (in which the displacement field is the flow of an autonomous dynamical system), starting from the initial position at $t = 0$ (here indicated with p_0, i.e., the position of the point before applying the deformation update u). This problem is solved efficiently by squaring recursively K times the transformation v (i.e., computing K times $v \circ v$) which is initialized as a rescaled version of u, i.e., $v = 2^{-K}u$, so that $\|v\|^2$ is small enough to get convergence (the smallest value of K for which $\|v\|^2 < 0.5$ was considered).

2.2.2. Multi-Image Demons

Demons algorithm was here generalized to the case of multiple data generated by processing the two images to be registered. The aim is to get a single deformation allowing to match optimally many pictures obtained from the source and target images. The method could be applied also in the case in which two sets of multiple images were taken using different sensors, but only under the assumption that the same deformation can map pairs of images from the two sets (otherwise, different methods, e.g., group-wise registration [22][34], should be applied). As this condition is difficult to be matched, from now on we assume that the multiple images were all obtained by pre-processing the two MRIs to be registered (notice also that this is one of the main innovations proposed here).

Specifically, assume that a target image F is processed by N processing algorithms obtaining a set of images $\{F_i\}$, where $i = 1, \cdots, N$; the source image M is processed by

the same algorithms obtaining the set $\{M_i\}$. We assume that the N pairs (F_k, M_k), for each k between 1 and N, can be registered by the same transformation s, to be estimated. As detailed below, the pre-processing techniques indicated in Figure 2 were considered for the application on MRIs.

The optimization problem to be solved to compute s is obtained generalizing equation (6) by summing more mean squared errors, one for each image pair

$$\underset{u}{\operatorname{argmin}} \sum_{k=1}^{N} \|F_k - M_k \circ s - J_k u\|^2 + \Sigma_k^2 \|u\|^2 \tag{14}$$

where J_k is the Jacobian of $M_k \circ s$ and $\Sigma_k = |F_k - M_k \circ s|$ is the regularization term that, as stated in Section 2.2.1, is chosen dependent on the registration error. The minimization problem is written in matrix form as follows

$$\underset{u}{\operatorname{argmin}} \left\| \begin{bmatrix} J_1 \\ J_2 \\ \vdots \\ J_N \\ \\ \Sigma_1 \\ \vdots \\ \Sigma_N \end{bmatrix} u - \begin{bmatrix} F_1 - M_1 \circ s \\ F_2 - M_2 \circ s \\ \vdots \\ F_N - M_N \circ s \\ 0 \\ \vdots \\ 0 \end{bmatrix} \right\|^2 \tag{15}$$

Normal equations are given by the following expression

$$\begin{aligned} \begin{bmatrix} J_1^T & \cdots & J_N^T & \Sigma_1^T & \cdots & \Sigma_N^T \end{bmatrix} \begin{bmatrix} J_1 \\ \vdots \\ J_N \\ \Sigma_1 \\ \vdots \\ \Sigma_N \end{bmatrix} u = \\ = \begin{bmatrix} J_1^T & \cdots & J_N^T & \Sigma_1^T & \cdots & \Sigma_N^T \end{bmatrix} \begin{bmatrix} F_1 - M_1 \circ s \\ F_2 - M_2 \circ s \\ \vdots \\ F_N - M_N \circ s \\ 0 \\ \vdots \\ 0 \end{bmatrix} \end{aligned} \tag{16}$$

The following update of the local displacement field solves these equations

$$u = \frac{\sum_{i=1}^{N} (F_i - M_i \circ s) J_i^T}{\sum_{i=1}^{N} \|J_i\|^2 + \Sigma_i^2} \tag{17}$$

Given the estimated displacement field, it is smoothed, converted into its diffeomorphic version and then applied to the source map to update it (as described in the previous section on classical demons algorithm).

In the following, this generalization of the demons algorithm to multiple images is referred to as the "multi-image algorithm". The algorithm is shown in Figure 3: multiple images are generated pre-processing the input pictures, then the deformation is obtained by iterating the application of equation (17), the composition by exponential map and the smoothing. The method is similar to the multi-channel diffeomorphic demons proposed in [21] to solve a 4D registration problem. However, notice that in [21] a voxel was associated to each channel. Moreover, the computation time was quite high and the application was different, as more channels were available and not generated by pre-processing the original images with different methods, as proposed here.

2.2.3. Balanced Multi-Image Demons

Another variation of the standard demons algorithm is also proposed. The standard algorithm deforms the source image and fits it over the target one. The deformed image is estimated by interpolation. However, in this way, the target image is kept whereas the source one is perturbed by the interpolation method used to estimate the deformations. In order to treat the two images in the same way, symmetric approaches were introduced in the literature [24][25]: a brief discussion of them is given in Appendix 1 and a comparison with the new proposed method is provided in the Results section.

A balanced approach is introduced here, in which, at each iteration, deformations are estimated and implemented in alternation to both the source and the target images[1]

$$u_F = \frac{\sum_{i=1}^{N}(F_i \circ \hat{s} - M_i \circ s)J_i^T}{\sum_{i=1}^{N}\|J_i\|^2 + \Sigma_i^2} \qquad u_M = \frac{\sum_{i=1}^{N}(M_i \circ s - F_i \circ \hat{s})\hat{J}_i^T}{\sum_{i=1}^{N}\left\|\hat{J}_i\right\|^2 + \hat{\Sigma}_i^2} \tag{18}$$

where u_F and u_M are the updates of the deformation of F and M, respectively; $\hat{s}$ is the estimated deformation to be applied to F; $\hat{J}_i$ and $\hat{\Sigma}_i$ are the Jacobian matrixes and the regularizations of the images $F_i \circ \hat{s}$ (notice that the expression for u_F is the same as that for u in equation (17), in which $\hat{s} = \mathbb{1}$).

In this way, the sets of target and source images are mapped on other ones (i.e., $F_i \circ \hat{s}$ and $M_i \circ s$), toward which the two sets converge. Thus, the theoretical solution of the problem is not unique. However, the algorithm obviously converges to a unique numerical solution, for which source and target images are treated in the same way. Finally, the deformation that transforms the source into the target image is computed as the composition of the two estimated deformations: the direct deformation starting from the first image is composed to the inverse of the deformation of the second (notice that such an inverse deformation can be computed, as the estimated transformations are diffeomorphisms).

In the following, the multi-image approach including also the further method discussed here is called "balanced multi-image algorithm". The algorithm is shown in Figure 3: after updating the deformation of $\{M_i\}$ (blocks indicated in black color), the

[1] This approach is referred to as symmetric in [4]. However, here it is called "balanced" to distinguish it from symmetric approaches proposed in the literature on demons.

deformation of $\{F_i\}$ is updated (blocks in gray color) and this is repeated for a selected number of iterations.

2.2.4. Tests of the registration algorithms

Three different methods are used to make the registration: the classical demons algorithm, its multi-image generalization and the balanced multi-image method. Two further symmetric algorithms (introduced in Appendix 1) are tested, to compare their performances with the balanced method. Finally, a deep convolutional neural network with UNet topology was developed to segment the brain in three regions (training was based on a dataset of 40 MRIs, i.e., the last images from [31], after removing the first 10 which are here used for test; refer to Appendix 2 for the details). It was used to compare the innovative method with a deep learning approach in the brain segmentation test.

The multi-image approaches (either balanced or not) are applied on 5 images. They were chosen on the basis of preliminary tests detailed in Appendix 3 and showed to provide useful non-redundant information, which could be applied in different conditions (e.g., noisy images or different gray scales). The 5 selected images are the original one and additional pictures obtained by processing it using the following operations: contrast-limited adaptive histogram equalization [35] (with diameter of the neighbors equal to 32 pixels), local median (with neighborhood of diameter 5 pixels), local entropy (with circular neighborhood of radius 15 pixels) and phase symmetry [36].

The registration methods were run in the same conditions, considering a 2-level implementation scheme [24] (with an initial registration on a coarse resolution obtained under-sampling the images with a factor 2) with 200 updates for each level (that in preliminary tests were found to be sufficient to reach convergence).

The algorithms have been implemented in MATLAB® (Inc., Natick, Massachusetts, USA, ver. 2019b; interpreted single core implementation).

3. Results

Figure 1 shows an example of MRI included in the tests. The original image is on the left; the noisy versions obtained by corrupting it with either additive Gaussian or speckle noise are then shown.

Figure 2 shows an MRI and the other images included in the multi-image versions of the demons algorithm.

Figure 3 shows a block diagram of the methods. The input pictures are first processed to compute the filtered images. Then the two sets of images are iteratively processed by three steps: estimation of the deformation update, use of the exponential map to get a diffeomorphism and Gaussian smoothing. These steps are applied only to the source images $\{M_i\}$ for 200 iterations by the multi-image method; the same steps are implemented in alternation to the sets of images target $\{F_i\}$ and source $\{M_i\}$ (100 iterations each) by the balanced multi-image algorithm.

Figure 4 shows an example of processing in a test on simulation. The source MRI (A) was deformed by a known deformation, obtaining the target image (B). Then the 3 algorithms registered the first (source) image over the second (target). The registrations estimated by the 3 algorithms (C-E) and the deformations (simulated and estimated, F-I) are shown. The mean squared errors in estimating the deformation are indicated.

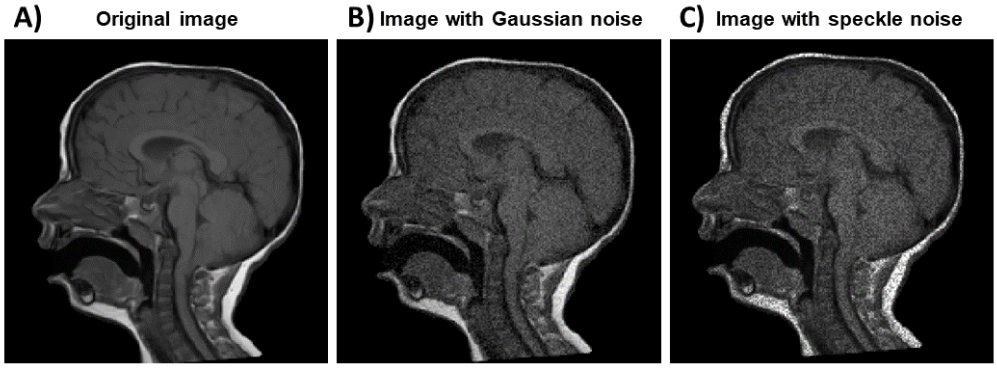

Figure 1: A) Example of original MRI used for the tests and the same image corrupted by either B) additive Gaussian or C) speckle noise.

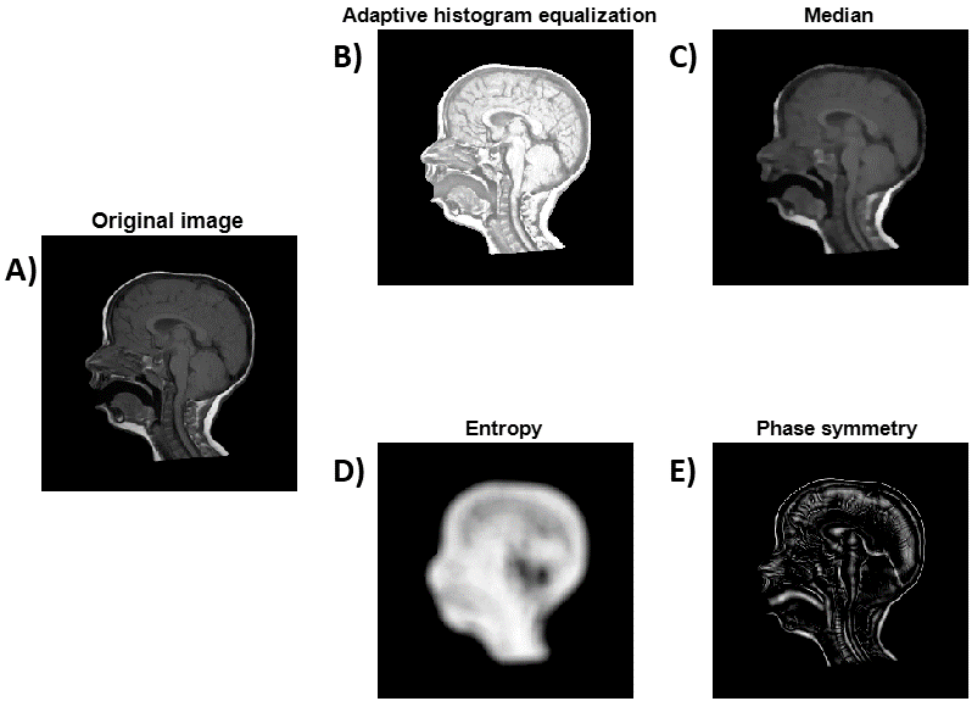

Figure 2: A) Same MRI as in Figure 1 and B)-E) the images used in the multi-image approaches, obtained by the following processing methods: B) adaptive histogram equalization (with diameter of the neighbors equal to 32 pixels), C) median filter (with neighbors of diameter 5 pixels), D) local entropy (circular neighbors with radius of 15 pixels) and E) phase symmetry.

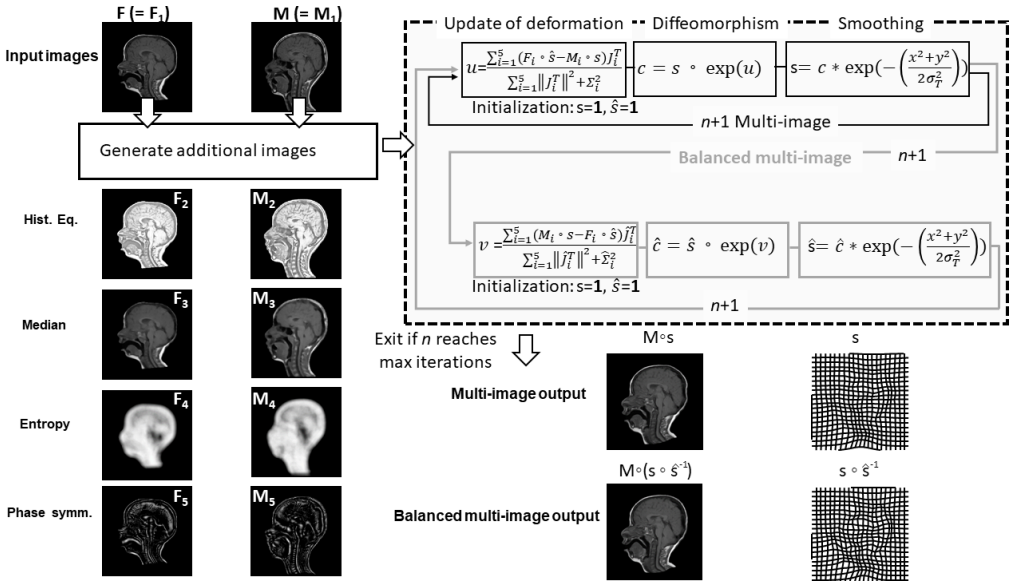

Figure 3: Block diagram of the multi-image and balanced multi-image methods. Both methods require to generate a set of images starting from the original input pictures. Then, deformation update, application of exponential diffeomorphism and Gaussian smoothing are iterated either only on the set of source images $\{M_i\}$ (multi-image algorithm, indicated in black), or in alternation to the set of source images $\{M_i\}$ and target images $\{F_i\}$ (balanced multi-image algorithm; the additional processing applied to the target images is indicated in gray color).

Notice that the multi-image approach allows to improve over the classical demons the estimation of the deformation and the balanced multi-image method provides a further improvement.

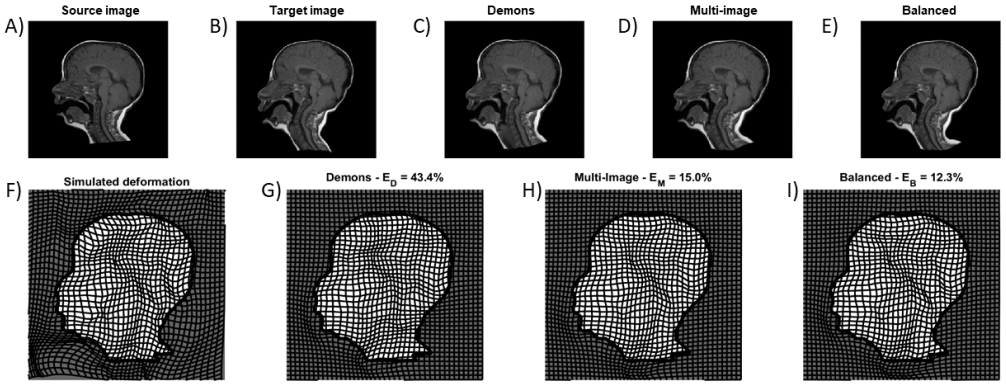

Figure 4: Processing of an MRI (same as in Figure 1). A) The original image is shown together with B) the deformed one and its estimations obtained by C) standard demons, D) multi-image and E) balanced multi-image approaches. Below, the deformations are shown, either F) simulated or G)-I) estimated by the 3 methods (E_D, E_M and E_B are the percentage mean squared errors in estimating the simulated deformation using the 3 methods, respectively, normalized with respect to its mean squared value; the deformation was considered only in the light region, which includes the head).

The indication provided by this figure is the same for all the tested simulated conditions: the multi-image approach improves the estimation of the deformation with respect to the classical demons algorithm and the balanced version gives a further improvement. Figure 5 shows the distributions of the errors for all cases (as box and whisker plots). The errors vary considering different images, but, as stated above, paired comparisons of same tested images (either original or corrupted by noise) processed by the different methods indicate that there are always improvements when using different approaches in the following order: classical demons algorithm, multi-image generalization and balanced multi-image method.

The algorithms were run on a PC with Intel® Core i7-7500U, Dual-Core, clock frequency of 2.7 GHz, 8 GB of RAM and 64 bits operating system. The computational time of a single registration was 24.8±1.6 s (mean±std) for the standard demons, 41.9±2.5 s for the multi-image algorithm (67.9±8.0% longer than the standard approach) and 54.5±2.2 s for the balanced multi-image method (116.1±16.2% longer than the standard demons). The larger computational cost with respect to the multi-image algorithm is due to the need of managing for each iteration two transformations (requiring to interpolate both images to apply their deformations).

Figure 6 shows an example of MRI and 10 different manual delineations of three regions of interest: brain, posterior fossa and cerebellum. The borders of the brain structures of interest were repeatedly indicated by an operator, using a custom made software in MATLAB® which allows to place some points which are then linearly interpolated to determine the boundary. The overlapping errors between pairs of delineations indicate a limit under which the measure of the performances of the algorithms is not reliable.

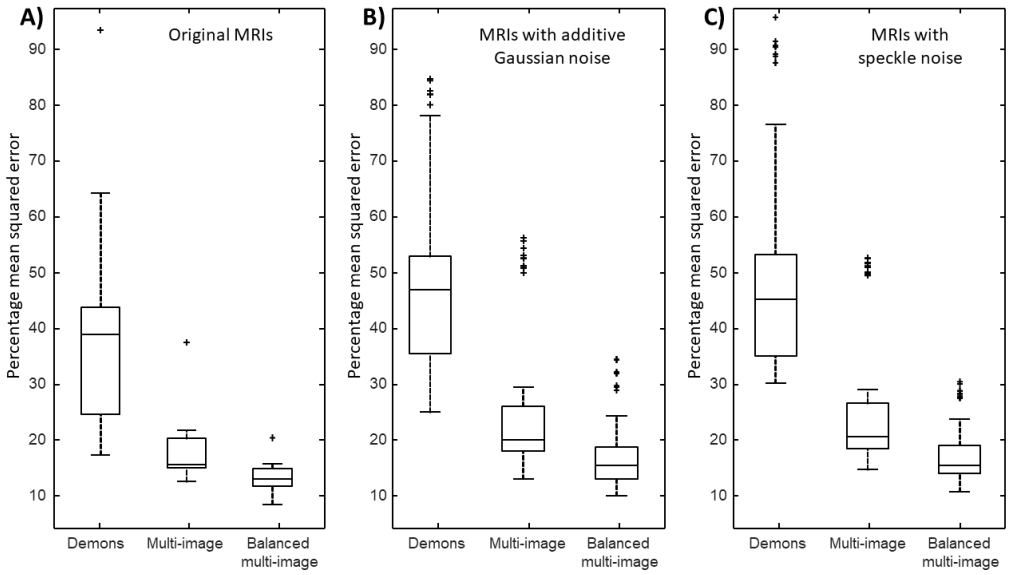

Figure 5: Box and whisker plots (indicating median, quartiles, range and outliers) of the errors in estimating the simulated deformation by the 3 methods (classical demons algorithm, multi-image generalization and balanced multi-image method) when applied to A) the original images or to those corrupted by either B) additive Gaussian or C) speckle noise.

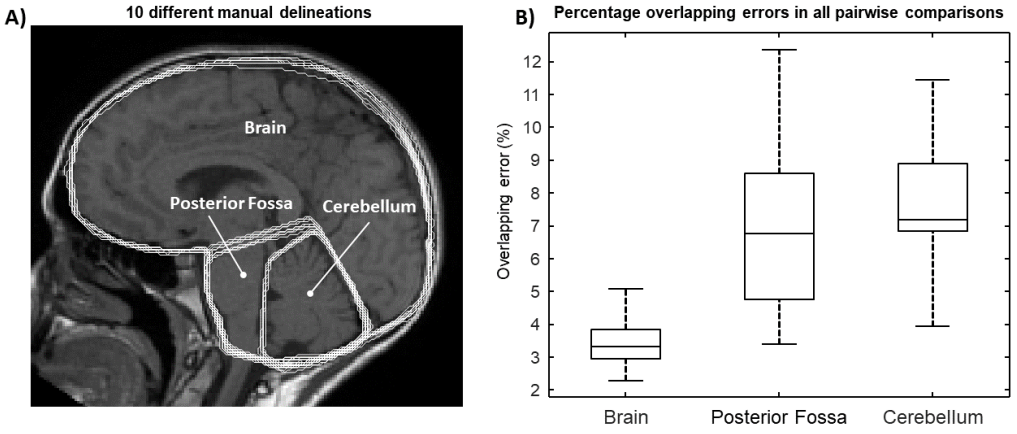

Figure 6: A) Different delineations of the regions of interest: brain, posterior fossa and cerebellum. B) Distributions of overlapping errors (box and whisker plot), defined as in Equation (1) and given as percentage of pixels with different classification (i.e., either included or excluded in a region) in all 45 pairs of manual delineations.

The performances of the algorithms in estimating the regions of interest are shown in Figure 7. The three regions were first delineated by an operator in each of the 10 MRIs; then, each MRI was used as atlas for the registration of the others, in order to estimate automatically those three regions in them. The paired Wilcoxon signed rank test indicates always an improvement when using multi-image approaches compared to the standard demons method. Moreover, a significant improvement is found when using the balanced approach instead of the multi-image only for estimating the cerebellum (even if an average reduction of the overlapping error of about 12% was observed also in the case of the brain and posterior fossa). Consider that, as indicated in Figure 6, the manual delineation has an inherent indeterminacy due to the limited resolution and the subjective nature of the procedure.

Figure 7D shows the processing times for a single registration by the different algorithms (run on the same PC mentioned above): 22.2±2.1 s (mean±std) for the standard demons, 34.0±2.1 s for the multi-image method (53.8±11.0% longer than standard, single-image demons) and 45.0±2.4 s for balanced multi-image technique (103.2±14.5% longer than standard demons).

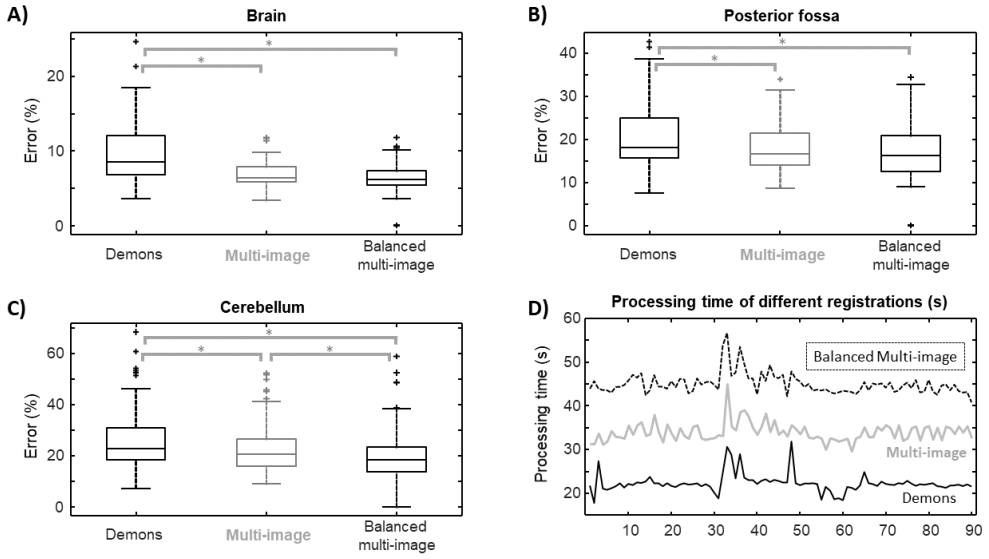

Figure 7: Test of region delineation by the atlas approach. Brain regions were manually delineated on all 10 MRIs. Each of them was used as atlas to estimate the regions on the other MRIs, each in turn considered as test (90 estimations were obtained). Distributions (box and whisker plot) of overlapping errors (defined as in Equation (1)) in identifying A) brain, B) posterior fossa and C) cerebellum. D) Computational time needed to process each case.

The balanced multi-image algorithm was also compared to the symmetric generalizations of demons introduced in Appendix 1. In brief, both approaches solve iteratively linearized optimization problems, updating the transformation with either of the following methods: 1. average of the forward and backward transformation mapping the source into the target image or vice-versa [24][25]; 2. solution of the linearized symmetric problem.

Both algorithms were applied on the entire dataset, considering the same number of updates as the other methods (thus, with an equivalent computational cost as the balanced multi-image algorithm). In the case of simulations, the errors in estimating the deformation were about 4.4% and 20% lower when using the balanced algorithm with respect to running either of the two symmetric methods, respectively. Statistically significant differences were indicated by the paired Wilcoxon signed rank test, with $p < 0.01$. When considering the experimental tests, the mean overlapping error in estimating posterior fossa and cerebellum regions manually delineated was about 1% and 2.7% lower when using the balanced approach instead of either of the two symmetric methods, respectively (statistically significant differences). No significant difference was found in estimating the borders of the brain.

Finally, the performances of the balanced multi-image algorithm in delineating brain, posterior fossa and cerebellum were compared to an UNet trained on 40 additional MRIs (details provided in Appendix 2). Different UNets were implemented. The median overlapping errors of the best UNet were 7.6%, 25.4% and 28.7%, for the three regions respectively. The median overlapping errors of the balanced multi-image algorithm were instead 7.5%, 21.9% and 22.3% (about the same as in Figure 7; notice that here the outliers were not removed). Notice that both the performances of the UNet and of the balanced multi-image method could be improved: indeed, the UNet could be trained on a larger database or the cost function could be upgraded by constraints (e.g., by enforcing each of the three regions to be connected or the topology to be preserved [37]); the balanced multi-image algorithm could be improved by a multi-atlas approach [27][28][29].

4. Discussion

A new approach is proposed for the non-rigid registration of two images. It merges information from multiple pictures extracted by pre-processing the images to be registered with different algorithms. In this way, each location of the pictures is augmented with additional information coming from its neighbor. Indeed, neighbors of each pixel are processed to extract averaged information or texture features. In this paper, 5 specific images have been selected as optimal for sagittal MRIs, after some tests in simulations (detailed in Appendix 3). Different pre-processing could be chosen to fit other applications. By changing the dimension of the neighbor, different spatial scales can be explored. Considering different processing operators, various local features (e.g., spectral or texture properties) can be included.

The specific implementation proposed here is based on the standard demons approach, but the same idea can be embedded in other registration algorithms. The new method has improved performances with respect to the standard demons, still keeping low the computational cost. The algorithm imposes that each image pair can be matched by using the same deformation[2]: this constraint allows to reduce the computational cost of the algorithm.

[2]Possibly, additional images could also be acquired by an experimental procedure involving the synchronous acquisition of more information from the investigated objects.

By considering multiple pairs of images obtained by filtering and texture operators, global information about a neighbor of each point is included to estimate the deformation. The integration of the information contained in the different images can make the registration more stable and accurate (obviously, if useful images are included). In the case of the classical demons algorithm, instead, the deformation is first computed separately for each pixel (considering only its intensity and local gradient); then, information from different pixels is merged relying simply on a Gaussian smoothing applied to the updated deformation.

In the literature, information from multiple images (taken by either different sensors or in different time instants) have been integrated to compute a non-rigid registration. For example, in the group-wise demons approach [22], more pictures are registered over an average image to be estimated. The method is more sophisticated than the one proposed here, but it has a higher computational cost. Moreover, the possibility of generating more pictures from the available ones, in order to get multi-scale/multi-modal information useful to improve the registration of single images, was not explored.

A further variation of the classical demons algorithm is also included here. The registration of the images is updated for each iteration of the algorithm in alternation to deform those from the source over those from the target image and then vice-versa (obtaining what is here called the balanced multi-image algorithm). In the literature, a similar method was introduced, that enforces demons algorithm to select a symmetric transformation [24][25]. As discussed in Appendix 1, two approaches can be considered: 1. computing the forward and backward transformations of the linearized problem and approximating the update as an average of them; 2. updating the transformation with the solution of the linearized symmetric optimization problem. Small improvements of the performances were obtained using the balanced instead of the symmetric methods. This can be possibly justified considering that the symmetric approaches impose constraints to the transformation, whereas the balanced algorithm searches for optimal solutions separately for the forward and backward problems. The improvements were larger when considering the simulated instead of the experimental conditions, the latter requiring the solution of a segmentation problem. Indeed, simulations provide ideal testing conditions, whereas manual delineation is affected by subjectivity and by an indeterminacy which limits the possibility of correctly measuring the accuracy: Figure 6 shows that an overlapping error of about 5% was found when delineating more times the brain regions on the same MRI.

Comparing the new algorithms with the standard demons, the tests indicate that the proposed algorithms improve the estimation of a simulated deformation applied to MRIs, either corrupted with noise or not. Specifically, the multi-image algorithm always performs better than the classical demons, with about a 50% of reduction of the error in estimating the simulated deformation. The balanced multi-image approach provides always the best performances, with an average error in estimating the deformation which is about the 36% of that of standard demons. Moreover, being aware of the subjective nature of manual delineation, the new algorithms are tested in an experimental problem of registration of pairs of MRIs. Again, the algorithms show significant improvements with respect to the standard demons: overlapping errors in the average are 15% and 29% lower, when using the multi-image and the balanced multi-image methods, respectively. The performances of the balanced multi-image approach in brain segmentation are also a bit superior in the average, but similar to those of a UNet (trained on a dataset of 40

images). Both algorithms could be improved, e.g., integrating information from multiple atlas to refine the delineation of the proposed registration approach and enlarging the dataset to better train the UNet: however, the results show that both methods are reasonable approaches for brain segmentation.

As a limitation, in this study only specific tests are shown and the simulated deformation is always the same[3]. Further tests are suggested for future studies (e.g., on other applications concerning different imaging techniques or on different registration methods embedding multiple images obtained by pre-processing the available data). However, the 300 registration tests performed in this study (210 simulations and 90 experimental delineations of brain regions) already indicate highly significant outcomes. Some additional segmentation results can be found in [31], where the same methods are applied on 50 MRIs.

Specific pre-processing techniques are considered to produce the additional images, which were chosen ad hoc for the application at hand. Each of them could provide some useful information in different conditions: for example, the adaptive histogram equalization is useful if images have different distributions of intensity (this could happen in the experimental tests, but not in the simulations shown here; however, some additional tests indicate that adaptive histogram equalization largely improves the estimation of a simulated deformation if the target image is also gamma corrected); the median filter is useful in the case of noisy data (for example, preliminary tests indicate that the use of the median filtered image largely improves the estimation of a simulated deformation if salt and pepper noise is included in the images). Thus, in different conditions, different pre-processing (e.g., extracting edges, texture features, global information from a neighbor of each pixel) could be important to improve the registration. The best set of images should be chosen on the basis of the specific application. Selecting automatically the best processing to generate the additional images could be an important future development. Another important future perspective could be the extension to 3D segmentation of the brain. Some interesting results have also been obtained using a deep learning approach [38][39]. The current 2D implementation is functional to the application we are currently interested in, namely the Chiari malformation, which is more evident in sagittal images [30][31].

5. Conclusion

An efficient generalization of demons method is proposed: the balanced multi-image algorithm. Its performances in each simulated test considered here are greater than those of the classical approach; statistically significant improvements are also found in a registration test (even if some uncertainty is present in that case, due to the subjective delineation of brain regions). The algorithm requires only a small additional computational cost with respect to the original method. Using more images, all extracted by pre-processing the single initial pictures to be registered, can be considered as a multimodal approach. Indeed, each operation providing a new image (e.g., extracting specific frequency components or texture information) summarizes in each location the result

[3]However, consider that a large deformation was simulated, obtaining a registration problem which is quite difficult, with respect to the matching of two different experimental MRIs.

of processing neighboring pixels around it. In this way, some local information on a neighbor is collected into a specific position. This paper shows that such an information can help in improving the registration, making it more accurate and robust to noise. Moreover, a balanced approach, in which forward and backward registrations are applied in alternation for each iteration of the algorithm, provides a further improvement of the performances (which are also slightly superior to those of other symmetric generalizations of demons applied to the same data).

Recent works show the application of this balanced multi-image algorithm to sagittal brain MRIs to extract morphometrics useful to identify the optimal surgical intervention to treat Chiari malformation [30][31].

It is expected that this method could find applications in different non-rigid registration problems. The idea of augmenting the local information by adding multiple images extracted from the pictures to be registered could also be beneficial for other registration approaches than demons. The integration of this approach in a multiple atlas registration strategy [27][28][29] is straightforward and could further improve the performances in delineating specific brain structures.

Appendix 1 - Symmetric registration approaches

A short introduction to symmetric demons algorithms is provided here. Some methods were introduced in the literature [24][25] and can be considered as alternatives to the balanced algorithm discussed in this paper.
The cost function to be minimized is the sum of the errors in computing the deformations mapping the source into the target images and vice-versa, imposing that an estimated deformation is the inverse of the other. Thus the following terms are included in the functional to be minimized

$$\|F(p) - M \circ s(p)\|^2 + \left\|M(p) - F \circ s^{-1}(p)\right\|^2 \tag{19}$$

where s^{-1} is the inverse transformation of s. Two approaches are considered to face this problem.

1. An approximate solution was proposed in [24][25], where updates in forward and backward direction, $u_{F\to M}$ and $u_{M\to F}$, were searched by minimizing the linearized error of mapping F into M and vice-versa, respectively. Then, the update for the map going from M to F was a linear combination of these two estimations: $u = (u_{M\to F} - u_{F\to M})/2$.
2. As the equations for the update are linear, a direct approach could solve in the least squared sense the problem of searching for a symmetric transformation (notice however that this method has not been used in the literature on demons, yet). For simplicity, consider the single image case:

$$\begin{aligned} &\|F(p) - M \circ s_* - J_M u\|^2 + \left\|M(p) - F \circ s_*^{-1} + J_F u\right\|^2 + \tfrac{\sigma_i^2}{\sigma_x^2}\|u\|^2 = \\ &= \left\| \begin{bmatrix} J_M \\ -J_F \\ \frac{\sigma_i}{\sigma_x} \end{bmatrix} u - \begin{bmatrix} F(p) - M \circ s_* \\ M(p) - F \circ s_*^{-1} \\ 0 \end{bmatrix} \right\|^2 \end{aligned} \tag{20}$$

where s_* is the deformation for this symmetric implementation of demons algorithm, J_M is the Jacobian of $M \circ s_*$ and J_F is the Jacobian of $F \circ s_*^{-1}$. The normal equations are

$$\begin{bmatrix} J_M^T & -J_F^T & \frac{\sigma_i}{\sigma_x} \end{bmatrix} \begin{bmatrix} J_M \\ -J_F \\ \frac{\sigma_i}{\sigma_x} \end{bmatrix} u = \begin{bmatrix} J_M^T & -J_F^T & \frac{\sigma_i}{\sigma_x} \end{bmatrix} \begin{bmatrix} F(p) - M \circ s_* \\ M(p) - F \circ s_*^{-1} \\ 0 \end{bmatrix} \tag{21}$$

The solution is

$$u = \frac{(F - M \circ s_*) J_M^T + (F \circ s_*^{-1} - M) J_F^T}{\|J_M\|^2 + \|J_F\|^2 + \frac{\sigma_i^2}{\sigma_x^2}} \tag{22}$$

with straightforward generalization in the case of multiple images.

Appendix 2 - A deep learning approach for brain segmentation

UNet is a deep neural network, including convolutional layers, with an architecture consisting of contraction, bottleneck and expansion sections (thus resembling a "U" topology, justifying its name) [40]. It is finding outstanding performances in semantic segmentation tasks [38][39][41][42].

Different multi-class networks were developed using the deep learning toolbox of MATLAB®. They were trained (10 fold crossvalidation using 40 MRIs), using stochastic gradient descent with momentum (SGDM) optimizer (with momentum equal to 0.9) and cross entropy loss. Among many different trials, the three most promising networks had the following parameters:

- 58 layers (encoder depth = 4), learning rate = 0.1;
- 46 layers (encoder depth = 3), learning rate = 0.01;
- same as the first one, but histogram equalization applied first on the input images.

Further optimization of the parameters and choice of loss functions/optimizers can be carried out to achieve slightly better performance. Few trials were also lead using Dice loss and augmentation, but they did not seem to result in a significant improvement.

The first network mentioned above provided overlapping errors in delineating brain, posterior fossa and cerebellum with median 13.3% (quartiles 11.0–17.3), 36.1% (24.8–43.1) and 33.4% (28.6–47.4), respectively.
The second one provided reliable estimations of the brain only, with overlapping error of 17.5% (quartiles 15.3–23.4).
The third network provided overlapping errors in delineating brain, posterior fossa and cerebellum with median 7.6% (quartiles 7.1–9.2), 25.4% (21.5–34.3) and 28.7% (22.0–39.2), respectively.

The best UNet was the third one. Its performances were compared with those obtained by the balanced multi-image approach considering in turn each of the MRI as atlas (and excluding the atlas for the comparison). In all 10 cases, the mean error in estimating each of the 3 regions was lower when using the balanced multi-image approach.

The same deep learning approach (i.e., encoder depth = 4, learning rate = 0.1 and histogram equalized images) was also used to develop single-class networks, to segment

respectively the brain, the posterior fossa and the cerebellum. The three UNets had the following overlapping errors, respectively: median 12.3% (quartiles 11.1–16.2), 31.6% (27.2–34.4) and 19.0% (16.3–24.9). The estimation of the brain and the posterior fossa was always superior when using the balanced multi-image method. The estimation of the cerebellum was equivalent with the UNet and the balanced multi-image approach (i.e., lower errors were found when using the registration considering some atlases, but not with others). Notice that, using a specific atlas, the estimation could be better or worst, in relation to the presence or absence of cerebellar hernia (indeed, our patients had Chiari malformation, with different extension of the herniation). Indeed, as the estimated transformation was a diffeomorphism, if the hernia was present in the test image but not in the atlas (or vice-versa), it could not be estimated correctly. A correction focused on the reconstruction of the hernia is discussed in [30][31].

Appendix 3 - Selection of best images for MRI registration

The 5 images used for this study were selected out of the following set.

1. Original,
2. contrast-limited adaptive histogram equalized (with diameter of the neighbors equal to 32 pixels) [35],
3. local median (with neighborhood of diameter 5 pixels) ,
4. local entropy (with circular neighborhood of radius 15 pixels),
5. phase symmetry [36],
6. Laplacian of the image (finite difference approximation),
7. gradient of the image (both components; second order finite difference approximation),
8. local range (with 3×3 neighborhood),
9. local standard deviation,
10. local skewness,
11. local kurtosis,
12. nine Laws texture features (to emphasize levels, edges, spots and ripples) [43],
13. three-class segmentation (by k-means),
14. level set segmentation with bias correction (3 sets) [44].

The original image was always included in the set. Then, a sequential forward selection was performed, by adding the image out of the set that allowed to get best average performances in estimating simulated deformations applied on two noise free MRIs. Additional images were included in the best set until performances improved. A few tests were also performed with noisy data, obtained perturbing the images to be registered by either gamma correction, salt and pepper or additive Gaussian noise. Equalization and median filter were found to be much important in such conditions.

Finally, to test if some of the 5 selected images could be removed, all possible combinations of 4 images were used to estimate a simulated deformation of the entire dataset of 10 MRIs (noise free conditions). Median errors were always lower when using the entire set of 5 images. Statistically significant degradation of the performances of the multi-image approach were indicated by the Wilcoxon signed rank test ($p<0.05$) when either the local entropy or the phase symmetry were removed. In the case of the balanced multi-image approach, images to be kept to avoid statistically significant reduction of performances were the adaptive histogram equalized, the local median and the phase symmetry.

Acknowledgements

The author is grateful to Dr. C. F. Carlino for providing the MRIs and to Dr. M. Muffoletto for the support for the deep learning approach.

References

[1] Z. Yang, T. Dan, Y. Yang, Multi-temporal remote sensing image registration using deep convolutional features, IEEE Access 6 (6) (2018) 38544–38555. doi:10.1109/ACCESS.2018.2853100.

[2] L. G. Brown, A survey of image registration techniques, ACM Comput. Surv. 24 (4) (1992) 325–376. doi:10.1145/146370.146374.

[3] W. R. Crum, T. Hartkens, D. L. G. Hill, Non-rigid image registration: theory and practice, in: Journal of Radiology - Imaging Processing Special Issue, Vol. 77, 2004, pp. S140–S153. doi:10.1259/bjr/25329214.

[4] A. Sotiras, C. Davatzikos, N. Paragios, Deformable medical image registration: A survey, IEEE Trans Med Imag 32 (7) (2013) 1153–1190. doi:10.1109/TMI.2013.2265603.

[5] A. Keszei, B. Berkels, T. Deserno, Survey of non-rigid registration tools in medicine, J Digit Imaging 32 (30) (2017) 102–116. doi:10.1007/s10278-016-9915-8.

[6] M. Jenkinson, S. Smith, A global optimisation method for robust affine registration of brain images, Med Image Anal 5 (2001) 143–156. doi:10.1016/s1361-8415(01)00036-6.

[7] B. Zitová, J. Flusser, Image registration methods: a survey, Image and Vision Computing 21 (2003) 977–1000. doi:10.1016/S0262-8856(03)00137-9.

[8] B. Fischer, J. Modersitzki, Ill-posed medicine—an introduction to image registration, Inverse Problems 24 (3) (2008) 034008. doi:10.1088/0266-5611/24/3/034008.

[9] P. Anbeek, K. Vincken, G. van Bochove, M. van Osch, J. van der Grond, Probabilistic segmentation of brain tissue in mr imaging, Neuroimage 27 (2005) 795–804. doi:10.1016/j.neuroimage.2003.10.012.

[10] K. Babalola, B. Patenaude, P. Aljabar, J. Schnabel, D. Kennedy, W. Crum, S. Smith, T. Cootes, M. Jenkinson, D. Rueckert, An evaluation of four automatic methods of segmenting the subcortical structures in the brain (erratum in neuroimage, 2010;49(1):1152), Neuroimage 47 (4) (2009) 1435–1447. doi:10.1016/j.neuroimage.2009.05.029.

[11] R. Brouwer, H. Hulshoff Pol, H. Schnack, Segmentation of mri brain scans using nonuniform partial volume densities, Neuroimage 49 (2010) 467–477. doi:10.1016/j.neuroimage.2009.07.041.

[12] B. Fischl, D. Salat, E. Busa, M. Albert, M. Dieterich, C. Haselgrove, A. van der Kouwe, R. Killiany, D. Kennedy, S. Klaveness, A. Montillo, N. Makris, B. Rosen, A. Dale, Whole brain segmentation: automated labeling of neuroanatomical structures in the human brain, Neuron 33 (3) (2002) 341–355. doi:10.1016/s0896-6273(02)00569-x.

[13] R. Heckemann, J. Hajnal, P. Aljabar, D. Rueckert, A. Hammers, Automatic anatomical brain mri segmentation combining label propagation and decision fusion, Neuroimage 33 (1) (2006) 115–126. doi:10.1016/j.neuroimage.2006.05.061.

[14] A. Klein, J. Andersson, B. Ardekani, J. Ashburner, B. Avants, M. Chiang, G. Christensen, D. Collins, J. Gee, P. Hellier, J. Song, M. Jenkinson, C. Lepage, D. Rueckert, P. Thompson, T. Vercauteren, R. Woods, J. Mann, R. Parsey, Evaluation of 14 nonlinear deformation algorithms applied to human brain mri registration, Neuroimage 46 (3) (2009) 786–802. doi:10.1016/j.neuroimage.2008.12.037.

[15] J. Wu, A. Chung, A novel framework for segmentation of deep brain structures based on markov dependence tree, Neuroimage 46 (4) (2009) 1027–1036. doi:10.1016/j.neuroimage.2009.03.010.

[16] J. Zhang, J. Wang, X. Wang, X. Gao, D. Feng, Physical constraint finite element model for medical image registration, PLoS One 10 (10) (2015) e0140567. doi:10.1371/journal.pone.0140567.

[17] T. Fu, Q. Li, J. Zhu, D. Ai, Y. Huang, H. Song, Y. Jiang, Y. Wang, J. Yang, Sparse deformation prediction using markov decision processes (mdp) for non-rigid registration of mr image, Comput Methods Programs Biomed 162 (2018) 47–59. doi:10.1016/j.cmpb.2018.04.024.

[18] L. Fang, L. Zhang, D. Nie, X. Cao, I. Rekik, S. Lee, H. He, D. Shen, Automatic brain labeling via multi-atlas guided fully convolutional networks, Med Image Anal 51 (2019) 157–168. doi:10.1016/j.media.2018.10.012.

[19] J.-P. Thirion, Image matching as a diffusion process: an analogy with maxwell's demons, Medical Image Analysis 2 (3) (1998) 243–260. doi:10.1016/S1361-8415(98)80022-4.

[20] Y. Wen, C. Xu, Y. Lu, Q. Li, H. Cai, L. He, Gabor feature-based logdemons with inertial constraint for nonrigid image registration, IEEE Transactions on Image Processing 29 (2020) 8238–8250. doi:10.1109/TIP.2020.3013169.

[21] J. Peyrat, H. Delingette, M. Sermesant, C. Xu, N. Ayache, Registration of 4d cardiac ct sequences under trajectory constraints with multichannel diffeomorphic demons, IEEE Trans Med Imag 29 (7) (2010) 1351–1368. doi:10.1109/TMI.2009.2038908.

[22] H. Lombaert, L. Grady, X. Pennec, J.-M. Peyrat, N. Ayache, F. Cheriet, Groupwise spectral log-demons framework for atlas construction, in: Medical Computer Vision (MCV'12) MICCAI workshop, 2012.

[23] S. Reaungamornrat, T. De Silva, A. Uneri, S. Vogt, G. Kleinszig, A. Khanna, J. Wolinsky, J. Prince, J. Siewerdsen, Mind demons: Symmetric diffeomorphic deformable registration of mr and ct for image-guided spine surgery, IEEE Trans Med Imag 35 (2016) 2413–2424. doi:10.1109/TMI.2016.2576360.

[24] T. Vercauteren, X. Pennec, A. Perchant, N. Ayache, Symmetric log-domain diffeomorphic registration: A demons-based approach, in: Proceedings of the 11th International Conference on Medical Image Computing and Computer-Assisted Intervention - Part I, MICCAI '08, Springer-Verlag, Berlin, Heidelberg, 2008, pp. 754–761. doi:10.1007/978-3-540-85988-8_90.

[25] H. Lombaert, L. Grady, X. Pennec, N. Ayache, F. Cheriet, Spectral log-demons: diffeomorphic image registration with very large deformations, International Journal of Computer Vision 107 (3) (2014) 254–271. doi:10.1007/s11263-013-0681-5.

[26] J. Bai, T. Trinh, K. Chuang, A. Qiu, Atlas-based automatic mouse brain image segmentation revisited: model complexity vs. image registration, Magn Reson Imaging 30 (6) (2012) 789–798. doi:10.1016/j.mri.2012.02.010.

[27] P. Aljabar, R. Heckemann, A. Hammers, J. Hajnal, D. Rueckert, Multi-atlas based segmentation of brain images: atlas selection and its effect on accuracy, Neuroimage 46 (3) (2009) 726–738. doi:10.1016/j.neuroimage.2009.02.018.

[28] X. Artaechevarria, A. Munoz-Barrutia, C. Ortiz-de Solorzano, Combination strategies in multi-atlas image segmentation: application to brain mr data, IEEE Trans Med Imaging 28 (8) (2009) 1266–1277. doi:10.1109/TMI.2009.2014372.

[29] S. Bao, C. Bermudez, Y. Huo, P. Parvathaneni, W. Rodriguez, S. Resnick, P. D'Haese, M. McHugo, S. Heckers, B. Dawant, I. Lyu, B. Landman, Registration-based image enhancement improves multi-atlas segmentation of the thalamic nuclei and hippocampal subfields, Magn Reson Imaging 59 (2019) 143–152. doi:10.1016/j.mri.2019.03.014.

[30] L. Mesin, F. Mokabberi, C. F. Carlino, Identification of optimal surgical intervention for chiari i malformation, 2019 IEEE Conference on Computational Intelligence in Bioinformatics and Computational Biology (CIBCB) (2019) 1–5.

[31] L. Mesin, F. Mokabberi, C. F. Carlino, Automated morphological measurements of brain structures and identification of optimal surgical intervention for chiari i malformation, IEEE Journal of Biomedical and Health Informatics, in press.

[32] V. Vercauteren, X. Pennec, A. Perchant, N. Ayache, Diffeomorphic demons: Efficient non-parametric image registration, NeuroImage 45 (1) (2009) 61–72. doi:10.1016/j.neuroimage.2008.10.040.

[33] Y. Wen, L. Hou, L. He, B. Peterson, D. Xu, A highly accurate symmetric optical flow based high-dimensional nonlinear spatial normalization of brain images, Magn Reson Imaging 33 (4) (2015) 465–473. doi:10.1016/j.mri.2015.01.013.

[34] W. Huizinga, D. Poot, J. Guyader, R. Klaassen, B. Coolen, M. van Kranenburg, R. van Geuns, A. Uitterdijk, M. Polfliet, J. Vandemeulebroucke, A. Leemans, W. Niessen, S. Klein, Pca-based groupwise image registration for quantitative mri, Med Image Anal. 29 (2016) 65–78. doi:10.1016/j.media.2015.12.004.

[35] K. Zuiderveld, Graphics gems iv, Academic Press Professional, Inc., San Diego, CA, USA, 1994, Ch. Contrast Limited Adaptive Histogram Equalization, pp. 474–485.

[36] P. Kovesi, Symmetry and asymmetry from local phase, in: Tenth Australian Joint Conference on Artificial Intelligence, 1997, pp. 2–4.

[37] X. Hu, F. Li, D. Samaras, C. Chen, Topology-preserving deep image segmentation, in: H. Wallach, H. Larochelle, A. Beygelzimer, F. d'Alché-Buc, E. Fox, R. Garnett (Eds.), Advances in Neural Information Processing Systems 32, Curran Associates, Inc., 2019, pp. 5657–5668.

[38] Ö. Çiçek, A. Abdulkadir, S. Lienkamp, T. Brox, O. Ronneberger, 3d u-net: Learning dense volumetric segmentation from sparse annotation, CoRR abs/1606.06650.

[39] E. Gibson, W. Li, C. Sudre, L. Fidon, D. Shakir, G. Wang, Z. Eaton-Rosen, R. Gray, T. Doel, Y. Hu,

T. Whyntie, P. Nachev, M. Modat, D. Barratt, S. Ourselin, M. Cardoso, T. Vercauteren, Niftynet: a deep-learning platform for medical imaging, Computer Methods and Programs in Biomedicine 158 (2018) 113–122. doi:10.1016/j.cmpb.2018.01.025.

[40] O. Ronneberger, P. Fischer, T. Brox, U-net: Convolutional networks for biomedical image segmentation, in: Medical Image Computing and Computer-Assisted Intervention (MICCAI), Vol. 9351 of LNCS, Springer, 2015, pp. 234–241.

[41] M. Havaei, A. Davy, D. Warde-Farley, A. Biard, A. Courville, Y. Bengio, C. Pal, P.-M. Jodoin, H. Larochelle, Brain tumor segmentation with deep neural networks, Medical Image Analysis 35 (2017) 18 – 31.

[42] X. Zhuang, L. Li, C. Payer, D. Štern, M. Urschler, M. P. Heinrich, J. Oster, C. Wang, Örjan Smedby, C. Bian, X. Yang, P.-A. Heng, A. Mortazi, U. Bagci, G. Yang, C. Sun, G. Galisot, J.-Y. Ramel, T. Brouard, Q. Tong, W. Si, X. Liao, G. Zeng, Z. Shi, G. Zheng, C. Wang, T. MacGillivray, D. Newby, K. Rhode, S. Ourselin, R. Mohiaddin, J. Keegan, D. Firmin, G. Yang, Evaluation of algorithms for multi-modality whole heart segmentation: An open-access grand challenge, Medical Image Analysis 58 (2019) 101537.

[43] K. Laws, Textured image segmentation, Ph.D. thesis, University of Southern California (1980).

[44] C. Li, R. Huang, Z. Ding, J. C. Gatenby, D. N. Metaxas, J. C. Gore, A level set method for image segmentation in the presence of intensity inhomogeneities with application to mri, IEEE Trans on Image Proc 20 (7) (2011) 2007–2016. doi:10.1109/TIP.2011.2146190.